

Supercell convergence of charge-transfer energies in pentacene molecular crystals from constrained DFT

David H. P. Turban

Cavendish Laboratory, 19 J.J. Thomson Avenue, Cambridge, CB3 0HE, UK.

Gilberto Teobaldi

*Stephenson Institute for Renewable Energy and Department of Chemistry,
The University of Liverpool, Liverpool, L69 7ZF, UK.*

David D. O'Regan

CRANN, AMBER, and School of Physics, Trinity College Dublin, Dublin 2, Ireland.

Nicholas D. M. Hine

Department of Physics, University of Warwick, Gibbet Hill Road, Coventry, CV4 7AL, UK.

(Dated: November 4, 2018)

Singlet fission (SF) is a multi-exciton generation process that could be harnessed to improve the efficiency of photovoltaic devices. Experimentally, systems derived from the pentacene molecule have been shown to exhibit ultrafast SF with high yields. Charge-transfer (CT) configurations are likely to play an important role as intermediates in the SF process in these systems. In molecular crystals, electrostatic screening effects and band formation can be significant in lowering the energy of CT states, enhancing their potential to effectively participate in SF. In order to simulate these, it desirable to adopt a computational approach which is acceptably accurate, relatively inexpensive, which and scales well to larger systems, thus enabling the study of screening effects. We propose a novel, electrostatically-corrected constrained Density Functional Theory (cDFT) approach as a low-cost solution to the calculation of CT energies in molecular crystals such as pentacene. Here we consider an implementation in the context of the ONETEP linear-scaling DFT code, but our electrostatic correction method is in principle applicable in combination with any constrained DFT implementation, also outside the linear-scaling framework. Our newly developed method allows us to estimate CT energies in the infinite crystal limit, and with these to validate the accuracy of the cluster approximation.

I. INTRODUCTION

Singlet fission (SF) is a multiple-exciton-generation process that is of great interest for potential applications in photovoltaics [1–3]. Crystalline pentacene is a material that exhibits highly efficient SF on an ultrafast timescale of around 80 fs [4]. The system has been investigated in a number of experimental [5–8], theoretical [9–13], and combined [14, 15] studies. Pentacene is a five-membered linear polyacene and forms molecular crystals with a characteristic ‘herringbone’ lattice (Fig. 1). Intermolecular charge-transfer (CT) states spanning nearest-neighbour molecules are thought to play a central role in the ultrafast SF process in pentacene and similar molecules [10, 16–18]. In molecular crystals, neighbouring pairs of molecules (dimers) undergoing charge-transfer are embedded in a complex molecular environment where screening and hybridisation effects are important.

Angular-momentum preserving CT states are difficult to access with experimental techniques as they are optically dark, making it challenging to measure accurate excitation energies [19, 20]. They also pose a challenge to electronic structure theory. For example, linear-response time-dependent DFT with local exchange is known to perform poorly on CT-like states, severely underestimat-

ing their energies [21]. This stems from the fact that local functionals are unable to describe the long-ranged electron-hole interaction correctly, a problem that is related to, and which compounds, the well-known band-gap error of the underlying ground-state DFT calculation. A possible remedy is the use of long-range corrected functionals with asymptotically correct exchange [22]. However, this comes at the expense of introducing additional parameters and of a greatly increased computational cost. It is thus desirable and timely to construct a low-cost method that scales well to large system sizes and complex environments, and which simultaneously describes the electrostatic and quantum mechanical features of CT states with reasonable accuracy.

In this work, we make use of constrained DFT (cDFT) [24–27] in combination with linear-scaling DFT (as implemented in the ONETEP code [28]), applying it to intermolecular charge-transfer in two nearest-neighbour dimers taken from the pentacene crystal structure. The cDFT method has been applied to a wide variety of molecular systems, to date, in the context of CT excitation energies [29–32], electronic couplings [33–35], electron transfer [36–39] and molecular dynamics [40, 41]. A largely unresolved issue in this context, however, is that of achieving supercell convergence of CT excitations in extended models suitable for capturing the screening and

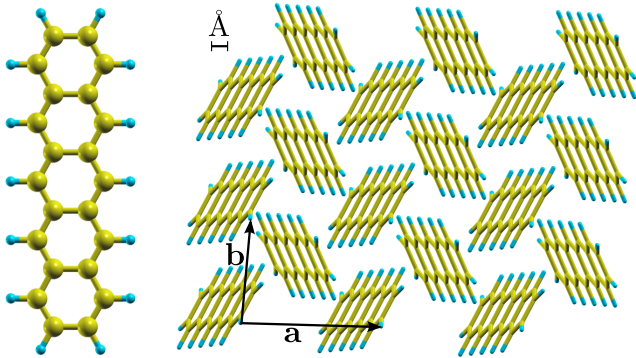


Figure 1. The pentacene ($C_{22}H_{14}$) single molecule and molecular crystal (S-phase [23]). The unit cell contains two molecules. The third lattice vector \mathbf{c} points out of the page.

hybridisation effects encountered in realistic systems. A solution to this problem, such as that which we presently propose, is then readily transferable to a range of complex systems of technological interest, not only in the context of photovoltaics, but also organic electronics [42–44] and spintronics [45].

We first calculate CT energies for the dimers in isolation, and we subsequently include screening effects by embedding such dimers in a small cluster of neighbours, and in supercells of the crystal. Supercell calculations allow us to approach the infinite limit using a correction scheme that eliminates the spurious dipole-dipole interactions between periodic images of the simulation cell. The only inputs required for this correction are the intrinsic dipole of the CT configuration and the dielectric tensor of the crystal. The latter is obtained from a density functional perturbation theory (DFPT) calculation [46]. We find that a single parameter, fit to the results of a series of calculations on different supercells, is sufficient to correct for the overestimation of electrostatic screening as a result of the aforementioned band-gap problem of DFT. The isolated calculations facilitate a comparison of the cDFT method with higher-level theory results from the literature [47]. In addition comparison between clusters and the infinite limit enables us to directly confirm the validity of the cluster approximation.

II. METHODS

A. The ground state: linear-scaling DFT

In order to carry out ground and excited state calculations on large clusters and supercells, we use linear-scaling DFT as implemented in the ONETEP code [28]. This LS-DFT methodology is based on the single-electron density matrix $\rho(\mathbf{r}, \mathbf{r}')$ rather than Kohn-Sham orbitals $\psi_i(\mathbf{r})$. The density matrix is expanded in a basis of

localised, atom-centred functions $\phi_\alpha(\mathbf{r})$ called NGWFs (non-orthogonal generalised Wannier functions) [48]:

$$\rho(\mathbf{r}, \mathbf{r}') = \sum_i \psi_i(\mathbf{r}) f_i \psi_i(\mathbf{r}') = \sum_{\alpha\beta} \phi_\alpha(\mathbf{r}) K^{\alpha\beta} \phi_\beta(\mathbf{r}'), \quad (1)$$

where $K^{\alpha\beta}$ is called the density kernel. The NGWFs are strictly truncated at a chosen localisation radius, which is a convergence parameter. The computational effort of traditional DFT methods, based on manipulation of Kohn-Sham eigenstates, inevitably scales as $\mathcal{O}(N^3)$, where N denotes the number of electrons. This is because there are $\mathcal{O}(N)$ eigenstates represented via $\mathcal{O}(N)$ basis functions, which have to be kept mutually orthogonal to $\mathcal{O}(N)$ other eigenstates. By contrast, in a density matrix representation, it is possible to achieve overall $\mathcal{O}(N)$ scaling if the density kernel is truncated at some cutoff radius such that it is a sparse matrix. This exploits the ‘near-sightedness’ of electronic structure in systems with a gap [49]. Instead of imposing orthogonality explicitly on Kohn-Sham states, it is necessary to constrain the density matrix to be idempotent and have a trace equal to the number of electrons N . In ONETEP, a nested loop optimisation scheme, utilising a conjugate gradients algorithm, is used to minimise the total energy with respect to both $K^{\alpha\beta}$ (subject to the constraints of idempotency and normalisation), and the set of NGWFs $\{\phi_\alpha(\mathbf{r})\}$. This approach has been shown to provide total energies and forces in $\mathcal{O}(N)$ effort with systematically controllable accuracy equivalent to that of a plane-wave basis [50]. This is possible despite using a minimal number of NGWFs (i.e., typically one per hydrogen atom, four per carbon atom), since the NGWFs are optimised in an underlying variational basis set of ‘psinc’ functions (delta functions with limited spectral range), which are fully equivalent to plane-waves.

B. Constrained DFT

In constrained DFT (cDFT) [24–26] the DFT total energy functional is augmented with terms that impose desired constraints on the charge (and/or spin) density of a system. While these constraints can take several forms, in this work we impose them using monomer-localised projection operators to partition the density. This gives a total functional of the form:

$$W = E_{\text{DFT}} + \sum_{\text{sites } I} V_I \left(\text{Tr}[\hat{P}_I \hat{\rho}] - N_I \right). \quad (2)$$

Here, the V_I are Lagrange multipliers that enforce occupancy targets N_I on specific sites in the system, which are defined via projectors \hat{P}_I . The sites in question may, generally, be atoms, groups of atoms or entire molecules. For example, if one aims to describe an intermolecular CT state, each of the two molecules involved constitutes a site. The Lagrange multipliers V_I act as artificial constraining potentials that cause charge to move around the

system (cf. Fig. 2a). These potentials are optimised *in-situ*, via a further conjugate gradients algorithm nested between kernel optimisation and NGWF optimisation, and iterated until the population targets N_I for the chosen sites are met. In the case of intermolecular CT states, these targets are, respectively, one fewer charge on the donor molecule and one additional charge on the acceptor, relative to the ground state.

Within the LS-DFT framework it is a natural choice to employ the aforementioned localised NGWFs to define site projectors [51]. In this work we employ a fixed set of NGWFs from a ground-state calculation for this purpose:

$$\hat{P}_I = \sum_{\alpha \in I} |\phi^\alpha\rangle \langle \phi_\alpha|, \quad (3)$$

where the sum $\alpha \in I$ refers to NGWFs centered on atoms belonging to site I . Here, subscript indices are used to describe the standard covariant functions $|\phi_\alpha\rangle$, while superscript indices refer to their contravariant duals $|\phi^\alpha\rangle$, which obey $\langle \phi_\alpha | \phi^\beta \rangle = \delta_{\alpha\beta}$. See Ref. [52, 53] for further discussion on this topic. A complication in the definition of site projection operators arises from the fact that the NGWFs are not orthonormal (this is true even of atomic orbitals, in the case of sites comprising more than one atom), meaning that the duals ϕ^α are not the same as the NGWFs. Instead, they are defined via the inverse of the NGWF overlap matrix $S_{\alpha\beta} = \langle \phi_\alpha | \phi_\beta \rangle$:

$$|\phi^\alpha\rangle = \sum_{\beta} |\phi_\beta\rangle (S^{-1})^{\beta\alpha}. \quad (4)$$

Given that the overlap and inverse overlap matrices can both be made sparse by appropriately-chosen truncation, it is possible to construct the inverse in linear-scaling computational effort using a sparse matrix implementation of Hotelling’s algorithm [54]. Duals constructed using the NGWF overlap matrix for the complete system are delocalised over that system, and thus present a highly undesirable choice for use in cDFT since this implies that constraining potentials V_I act non-locally on the charge density, with donor and acceptor subspaces overlapping. Appropriate localisation of the duals, to the region of the system of interest for defining a site, is achieved by suitably truncating the NGWF overlap matrix before its inversion, and then defining subspace duals for the purposes of building the site projection operators via the resulting subspace inverse overlap matrix $O_{\alpha\beta}$ instead of the full $S_{\alpha\beta}$, as described in [55]. Specifically, a ‘site-block’ scheme is imposed on the sparsity of the NGWF overlap matrix before it is inverted. Here, a block is defined by all NGWFs associated with a given site. Overlap matrix elements between NGWFs associated with different sites are set to zero (cf. Fig. 2b). Once this matrix has been inverted, it retains the same block pattern of sparsity, meaning that subspace duals are defined as a linear combination of only those NGWFs on the same constraint site.

When the sites are defined in self-contained manner, thereby, bi-orthogonality is unavoidably lost between

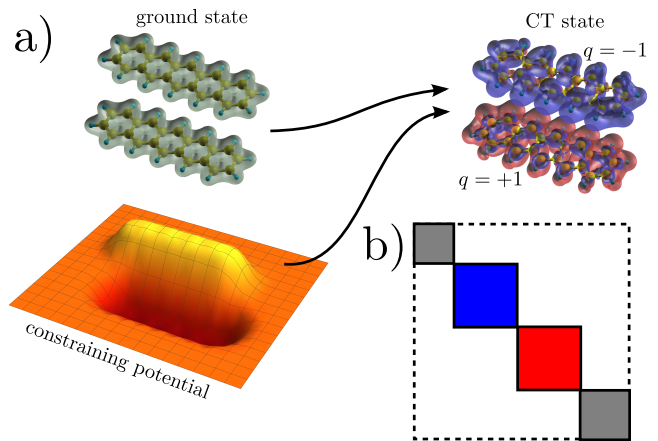


Figure 2. a) Schematic of the cDFT scheme used in this work: A nonlocal constraining potential (illustrated by 2D potential energy surface) constructed from atom-centred functions is applied to the single-electron density matrix. This causes charge to redistribute to obey chosen population constraints, and allows the description of CT excitations within the framework of standard DFT. b) Block scheme of truncated NGWF overlap matrix to ensure site-localisation of contravariant duals. Blue and red denote the constrained sites, gray the remaining system.

NGWFs and duals localised to different sites, in the event that these sites overlap to some degree. This carries the disadvantage the sum of charges over a set of such sites, covering the system, may not equal the true total charge. For well-separated donor and acceptor regions such as in the system at hand, any overestimation of site charge due to the latter effect is insubstantial in comparison to the dramatic overestimation incurred by using delocalised duals. On the other hand, even when the donor and acceptor regions do overlap substantially, unlike methods employing fully delocalized duals our approach ensures that the constraining potentials remain fully localised to their respective regions, with a smooth, non-oscillatory transition at the boundary.

A different approach to cDFT in the context of linear-scaling has been described in Refs. [56, 57].

In order to obtain energies of CT excitations, we first perform a ground state DFT calculation. This yields both a total energy for the ground state and a set of converged ground-state NGWFs which are subsequently used as cDFT projectors. To define the population targets for the cDFT run we simply add ± 1 to the ground state populations of the appropriate sites (acceptor: $+1$; donor: -1). The difference between the constrained total energy and the ground state energy yields the (vertical) CT excitation energy. Since we are interested in ultrafast processes like singlet fission where nuclear relaxation in the excited state is less significant, we restrict our attention to vertical excitation energies. In general, a geometry optimisation in the excited state would be required in order to correctly describe longer-lived CT states.

C. Computational Details

For all calculations we employ the LDA functional and norm-conserving pseudopotentials. The energy cutoff is chosen as 750 eV. We use 1 NGWF per hydrogen atom and 4 NGWFs per carbon atom. For the localisation radius of the NGWFs a value of 10 Bohr is chosen. Using these parameters the total energy is converged to 1 meV/atom at 10 Bohr NGWF radius compared to 14 Bohr, and to around 25 meV/atom at 750 eV cutoff compared to 1250 eV. All NGWFs are initialised to pseudoatomic orbitals [58] and then optimised in-situ in terms of the underlying psinc basis. The density kernel $K^{\alpha\beta}$ is not truncated in this work as all systems are small enough that sparse matrix algebra is only a minor component of the total computational effort. For the later Density Functional Perturbation Theory calculations, we utilise the CASTEP plane-wave DFT code [59] with the same pseudopotentials and cutoff energy. The DFPT calculations are performed with 12 k-points, corresponding to a maximum k-point spacing of 0.05 1/Å.

The S-phase molecular crystal structure considered here has two molecules per primitive cell and triclinic ($P-1$) space group symmetry. The lattice parameters are given by $a = 7.90$ Å, $b = 6.06$ Å, $c = 16.01$ Å, and $\alpha = 101.9^\circ$, $\beta = 112.6^\circ$, $\gamma = 85.8^\circ$ [60]. Optimised molecular geometries are taken from Ref. [23] in order to facilitate comparison of our calculations with Ref. [47] where high-level CASPT2/CASSCF and GW/BSE calculations were performed using the same geometries.

For calculations on isolated dimers and clusters we employ open boundary conditions. This is achieved by putting the dimers in a large simulation box and truncating the Coulomb interaction at large distances to eliminate electrostatic interactions between periodic images [61]. The calculations on supercells of the pentacene crystal use periodic boundary conditions.

III. DIMER & CLUSTER CALCULATIONS

The molecular geometries of the ‘herringbone’ dimer and the ‘parallel’ dimer are shown in Fig. 3. The herringbone dimer represents the unit cell of the pentacene crystal. While the long axes of the molecules are mostly aligned, there is a rotational offset around the same long axis between the units. In particular, this means that the two units in the herringbone dimer are not related by symmetry.

In the parallel dimer, on the other hand, the pentacene molecules belong to the same sublattice of the crystal and are related by a translation along lattice vector \mathbf{b} (cf. Fig. 1). As a result the molecular planes of the molecules are parallel. The translational correspondence together with the inversion symmetry of single pentacene molecules mean that the parallel dimer has an inversion centre, i.e. the units are symmetry-equivalent.

Configuration	our method	CASPT2/CASSCF	GW/BSE
Herringbone 1	2.04	2.22 [47]	1.92 [47]
Herringbone 2	2.72	2.55 [47]	2.60 [47]
Parallel	2.61	3.03 [47]	2.45* [47]

Table I. CT energies (eV) of isolated dimers, comparing our results with higher-level theory. The authors of Ref. [47] identify the excitation marked by an asterisk as a third locally excited state dominated by transitions between the frontier orbitals of the monomers. However, in a dimer there can only be two states of this kind. Hence, we concluded that the excitation does in fact have CT character.

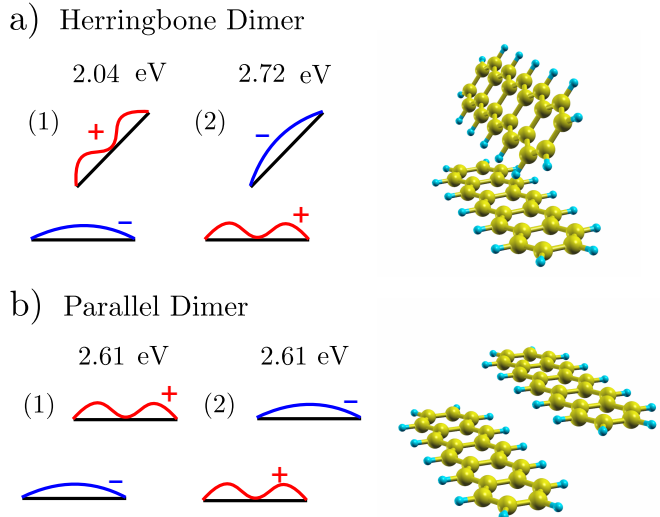


Figure 3. Dimer geometries and CT excitation energies from cDFT (quoted in eV). The significant energy gap between the two CT states in the herringbone dimer can be rationalised by considering the different charge distributions of electron and hole, and the geometry. The hole orbital corresponds to the pentacene HOMO which has a node on the long axis of the molecule. The electron orbital (LUMO), on the other hand, does not feature such a node. The partial alignment of the upper molecule with the dipole vector means that the bimodal charge distribution on the upper molecule has a lower Coulomb energy in configuration 1 as compared to configuration 2. In the parallel case the two CT states are related by inversion symmetry and the energies are degenerate.

First, we obtain CT energies for the dimers in isolation. The results are summarised in Fig. 3. The most striking aspect is the significant energy gap between the two CT configurations in the herringbone dimer due to their symmetry-inequivalence, as elaborated in the figure. In the parallel configuration the energies are degenerate due to inversion symmetry. The excitation energies for the herringbone configuration are within ~ 0.2 eV of literature values obtained with higher-level methods (cf. Table I). For the parallel configuration the discrepancy may be as large as ~ 0.4 eV, depending on the method compared to.

We next perform cluster calculations where we sur-

Configuration	isolated (2 mol)	4-mol cluster	10-mol cluster
Herringbone 1	2.04 (0.80)	2.16 (0.73)	2.00 (0.68)
Herringbone 2	2.72 (0.80)	2.25 (0.73)	2.04 (0.68)
Parallel	2.61 (1.13)	2.35 (0.92)	2.10 (0.87)

Table II. Comparison of CT states for isolated dimers and clusters. The table quotes the excitation energy of the CT state and the HOMO-LUMO gap of the ground state configuration in brackets (in units of eV).

round the dimers with a small cluster of neighbouring molecules fixed in the geometry of the molecular crystal (Table II). The 4-molecule clusters (144 atoms) only include the CT pair and the two shared nearest-neighbour molecules in the **a-b**-plane. In the 10-molecule clusters (360 atoms), all nearest-neighbour molecules in the **a-b**-plane are included. The results are summarised in Table II. We observe a significant down shift of the mean energy and closing of the relative gaps as the size of the cluster increases. This is driven by a reduction of the gap due to the hybridisation and increased electrostatic screening by neighbouring molecules. It should be noted that the degeneracy of the two parallel dimer CT states is very slightly lifted in the clusters (which does not exhibit exact inversion symmetry), but only within the quoted accuracy. Therefore, we only give a single value for the CT energy.

From the presented set of calculations alone it is difficult to determine whether sufficient convergence to the infinite limit has been reached with the 10-molecule cluster.

IV. SUPERCELL CALCULATIONS

We now consider the dimers embedded not in vacuum, but in the natural environment of the molecular crystal. This immediately raises the issue of treating a non-periodic, infinite system in DFT. In practice, one has to use supercell calculations with periodic boundary conditions. However, these suffer from finite-size errors which are particularly pronounced in the case at hand, as can be seen from the large scatter of 0.1-0.3 eV of the uncorrected CT energies in Fig. 4 (blue bars). This is a consequence of the large dipole moments of the CT configurations, resulting in significant dipole-dipole interactions between periodic images. The problem is expected to be even more pronounced in systems with either larger CT-dipoles, like biological photo-reaction centres, or smaller polarisabilities (e.g. due to smaller pi-systems).

We address this problem by deriving an energy correction that cancels the spurious interactions. We apply this correction to a range of calculations using supercells of varying shapes and sizes to demonstrate consistency of the method. The largest supercell considered has dimensions $3 \times 3 \times 2$, or 18 unit cells (1368 atoms).

Dipole-dipole correction

Periodic DFT codes employ the Ewald formula [62] to evaluate the electrostatic energy. The central idea is a splitting of the solution of Poisson's equation $\Delta\varphi = -4\pi\rho$ into parts that converge rapidly in real and reciprocal space, respectively. The splitting is controlled by an inverse length scale η , called Ewald's parameter.

If metallic boundary conditions are used (i.e. vanishing surface term), as is commonly the case, the total energy of an isolated system with a net dipole converges relatively slowly ($\sim V_{\text{cell}}^{-1}$) with the size of the simulation cell due to dipole-dipole interactions between periodic images. Makov & Payne showed that a better degree of convergence ($\sim V_{\text{cell}}^{-5/3}$) can be achieved by subtracting a dipole term from the Ewald energy [63]:

$$E_{\text{dip}} = -\frac{2\pi}{3V_{\text{cell}}} \cdot \mathbf{P}^2, \quad (5)$$

where \mathbf{P} is the total dipole moment of the simulation cell. The Makov & Payne result is only valid for cubic cells. If the aperiodic system to be studied is embedded in an isotropic dielectric one can apply the phenomenological approach by Leslie & Gillan [64]. Here the dipole-dipole interaction is reduced by the dielectric constant of the dielectric, i.e.

$$E_{\text{dip}} = -\frac{2\pi}{3V_{\text{cell}}} \cdot \frac{|\mathbf{P}|^2}{\epsilon}. \quad (6)$$

In order to be useful for CT states in pentacene supercells it is necessary to generalise these results to arbitrary cell shapes and, crucially, anisotropic dielectrics [65–67]. To achieve the first step we can employ the following expression by Kantorovich which is valid for general periodic cells and can be obtained by evaluating the Ewald formula for a periodic lattice of point dipoles [68]:

$$E_{\text{dip}} = -\frac{2\eta^3}{3\sqrt{\pi}} \cdot |\mathbf{P}|^2 + \frac{1}{2} \sum_{\alpha,\beta} P_{\alpha} \psi_{\alpha\beta} P_{\beta}, \quad (7)$$

where η is Ewald's parameter, and

$$\psi_{\alpha\beta} = \frac{4\pi}{V_{\text{cell}}} \sum_{\mathbf{k} \neq 0} \frac{k_{\alpha} k_{\beta}}{|\mathbf{k}|^2} e^{-|\mathbf{k}|^2/4\eta^2} - \eta^3 \sum_{\mathbf{l} \neq 0} H_{\alpha\beta}(\eta\mathbf{l}), \quad (8)$$

where \mathbf{k} denotes reciprocal lattice vectors, and \mathbf{l} denotes direct lattice vectors. Furthermore, we have

$$H_{\alpha\beta}(\mathbf{y}) = -\delta_{\alpha\beta} h(|\mathbf{y}|) + \frac{y_{\alpha} y_{\beta}}{|\mathbf{y}|^2} \left[3h(|\mathbf{y}|) + \frac{4}{\sqrt{\pi}} e^{-|\mathbf{y}|^2} \right], \quad (9)$$

with

$$h(y) = \frac{2}{\sqrt{\pi}} \cdot \frac{e^{-y^2}}{y^2} + \frac{\text{erfc}(y)}{y^3}. \quad (10)$$

If the dipoles are embedded in an anisotropic dielectric we need to modify Poisson's equation by substituting $\Delta \rightarrow \nabla^t \underline{\underline{\epsilon}} \nabla$, where $\underline{\underline{\epsilon}}$ is the dielectric tensor of

the medium. Now it turns out that in order to preserve the structure of the Ewald formula it is necessary to split the charge distribution anisotropically. This is achieved by inserting the inverse dielectric tensor in the exponential of the Gaussian smearing function, namely $\exp(-\eta^2|\mathbf{r}|^2) \rightarrow \exp(-\eta^2\mathbf{r}^t\boldsymbol{\underline{\underline{\epsilon}}^{-1}\mathbf{r})/\sqrt{\det\boldsymbol{\underline{\underline{\epsilon}}}}$. Using this substitution the solution of the (real space) Poisson equation for the smeared charge can be reduced to the isotropic case by a change of variables. In the reciprocal space term the denominator transforms in conjunction with the Poisson equation as $|\mathbf{k}|^2 \rightarrow \mathbf{k}^t\boldsymbol{\underline{\underline{\epsilon}}}\mathbf{k}$. In addition, the Fourier transform of the modified Gaussian smearing function is now given by $\exp(-\mathbf{k}^t\boldsymbol{\underline{\underline{\epsilon}}}\mathbf{k}/4\eta^2)$.

All in all, a structurally identical expression for the dipole contribution is obtained, the only difference being an overall factor of $1/\sqrt{\det\boldsymbol{\underline{\underline{\epsilon}}}}$ and linear transformations of the direct and reciprocal vectors:

$$\mathbf{P} \rightarrow \underline{\underline{D}}^{-1}\underline{\underline{C}}^t\mathbf{P}, \quad (11)$$

$$\mathbf{1} \rightarrow \underline{\underline{D}}^{-1}\underline{\underline{C}}^t\mathbf{1}, \quad (12)$$

$$\mathbf{k} \rightarrow \underline{\underline{D}}\underline{\underline{C}}^t\mathbf{k}. \quad (13)$$

Here $\underline{\underline{C}}$ is the (orthogonal) principal axis transformation that diagonalises $\boldsymbol{\underline{\underline{\epsilon}}}$, and $\underline{\underline{D}} = \text{diag}(\sqrt{\epsilon_1}, \sqrt{\epsilon_2}, \sqrt{\epsilon_3})$ with the eigenvalues ϵ_i of $\boldsymbol{\underline{\underline{\epsilon}}}$, i.e. $\boldsymbol{\underline{\underline{\epsilon}}} = \underline{\underline{C}}\underline{\underline{D}}^2\underline{\underline{C}}^t$ [69]. We note that transforming the lattice vectors in this way necessarily entails a rescaling of the cell volume, namely $V_{\text{cell}} \rightarrow V_{\text{cell}}/\sqrt{\det\boldsymbol{\underline{\underline{\epsilon}}}}$.

Applying the correction

First, we perform a DFPT calculation using the CASTEP code to obtain the dielectric tensor for the primitive cell of the pentacene crystal:

$$\boldsymbol{\underline{\underline{\epsilon}}}_{\text{DFPT}} = \begin{bmatrix} 3.48 & -0.18 & -0.12 \\ -0.18 & 3.14 & 0.19 \\ -0.12 & 0.19 & 5.61 \end{bmatrix}.$$

The actual dielectric tensor is assumed to be obtained by a uniform scaling $\boldsymbol{\underline{\underline{\epsilon}}} = c \cdot \boldsymbol{\underline{\underline{\epsilon}}}_{\text{DFPT}}$. The scaling accounts for the overestimation of screening due to the band-gap error, as previously discussed. By using a single scaling parameter c we employ the simplifying assumption that the overscreening of DFPT is isotropic. The dipole moments were taken from dimer cDFT calculations in vacuum (atomic units):

$$\mathbf{P}_{\text{her1}} = (1.45, -6.70, -2.07)^t, \quad |\mathbf{P}_{\text{her1}}| = 7.16$$

$$\mathbf{P}_{\text{her2}} = (-1.19, 7.58, 2.33)^t, \quad |\mathbf{P}_{\text{her2}}| = 8.02$$

$$\mathbf{P}_{\text{par1/2}} = \pm(-7.89, 4.23, 1.85)^t, \quad |\mathbf{P}_{\text{par1/2}}| = 9.14$$

The dipole correction is applied to the supercell energies as follows:

$$E_{\text{tot}} = E_{\text{cDFT}} - E_{\text{dip}}. \quad (14)$$

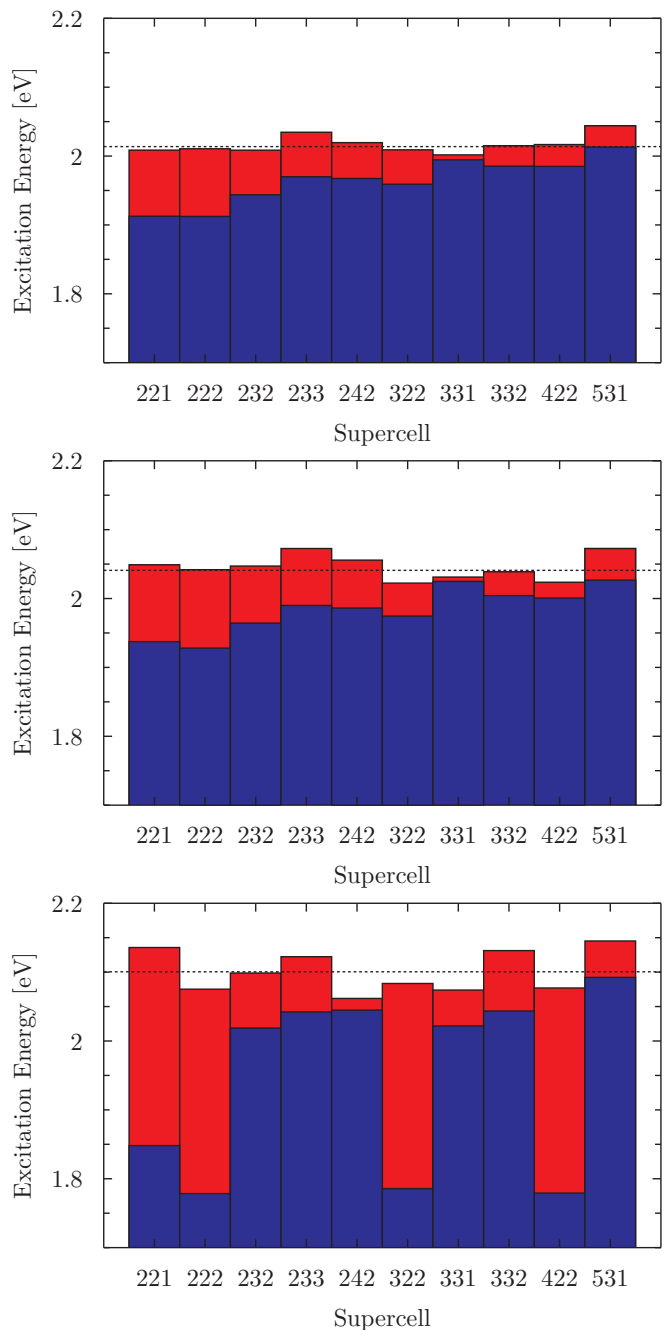


Figure 4. (Top) Herringbone 1 (Centre) Herringbone 2 (Bottom) Parallel. Uncorrected energies (blue) and dipole corrections (red) for CT states across a range of supercell embeddings. Dashed lines indicate corrected mean energies. Note that the dipole correction is negative for the 531 supercell for both herringbone configurations.

Minimising the combined standard deviation across all three dimer configurations yields a best-fit value $c = 0.378$. The effect of the correction using this value of c for the three cases is shown graphically in Fig. 4. We note that the value of c is in approximate agreement with the ratio of the DFT gap of ~ 0.8 eV and to the quasiparticle

gap of ~ 2.4 eV calculated with many-body perturbation theory [23], as might be expected.

Having applied Eq. (14), for the herringbone dimer we obtain a corrected mean energies of 2.01 eV and 2.04 eV, respectively. The parallel dimer yields a mean energy of 2.10 eV. The spread of corrected energies is down to 0.03-0.08 eV, a reduction by a factor of 3-4, demonstrating the success of the method. The significantly larger spread of values in the parallel dimer compared to the herringbone dimer is a result of enhanced dipole interaction between periodic images. This is due to the fact that the dimer (and hence dipole) is aligned with the crystal lattice (along lattice vector \mathbf{b} , cf. Fig. 1).

V. DISCUSSION

As elaborated above, the empirical parameter c in the method accounts for the overscreening of DFPT with local functionals. There are additional uncertainties due to the fact that the separation of periodic images is small, implying that the supercell calculations still exhibit a relatively high density of electron-hole pairs. This can modify the dielectric properties. Further errors may stem from higher-order electrostatic corrections as a result of the fact that the CT configurations considered take up a significant portions of the supercells and hence do not constitute perfectly point-like dipoles. All these effects are integrated in the c parameter. The remaining spread of energies is presumably related to residuals of these sources of error which cannot be eliminated with the single c parameter.

It is apparent that the dipole-corrected energies are essentially degenerate with those obtained for the 10-molecule cluster, within the quoted precision of 10 meV (cf. Table II). Presuming this holds for still-larger clusters, this result demonstrates the validity of the cluster approximation for molecular crystals of pentacene and likely a range of similar molecules (eg. tetracene). In case where the molecular unit of a molecular crystal has a net dipole, the cluster approach in vacuum would incur significant difficulties due to the unscreened net-dipole [70]. The current approach, in employing periodic boundary conditions, would not encounter such problems.

We observe that aggregation has a twofold effect on CT energies in the pentacene molecular crystal: an overall downshift, and an assimilation of the different CT configurations considered. The latter is particularly striking in the herringbone dimer, where the initial splitting of nearly 0.7 eV in isolation is reduced to only a few 10 meV when embedded in the crystal. Interestingly, the alignment of the three CT energies also changes. In the isolated dimers, the parallel CT energy is situated between the two herringbone energies, whereas in the crystal the parallel energy is slightly above the two (now nearly degenerate) herringbone energies.

We also note that although our calculations employ the computationally cheap LDA functional they do not

appear to suffer from a systematic underestimation of excitation energies relative to those calculated with higher levels of theory. This observation can be rationalised by noting that in cDFT the excited electron orbital is fully occupied. No DFT eigenvalues of unoccupied orbitals which are subject to large systematic underestimation enter the calculation. TDDFT with local exchange requires computationally expensive and parameter-dependent range-separated hybrid functionals in order to yield CT energies that are not severely underestimated [21, 22]. By contrast, using the novel combination of linear-scaling methodology with projector-based cDFT, we are able to perform relatively cheap calculations which scale well to large system sizes (1368 atoms, in this work).

We further note that the relatively low CT energies in the crystal of just above 2 eV put them on the lower end of experimental estimates [19]. They are in line with previous theoretical results indicating a significant admixture of CT-like components into the lowest singlet exciton in pentacene [71–73]. The low energies also lend support to the notion that a CT-mediated ‘superexchange’ mechanism can play a crucial role in ultrafast fission [10, 16–18].

Our procedure should also be transferable to other systems in which CT states are situated in a complex screening environment. These include (but are not limited to) a variety of organic materials for organic photovoltaics and optoelectronics/spintronics.

At this point there remain a number of limitations that need to be addressed by future work. Our method as presented in this work relies on the system in question exhibiting sufficiently homogeneous dielectric properties which can be approximated by a single dielectric tensor. Furthermore, the cDFT approach necessitates prior knowledge of the excited state structure such that appropriate donor and acceptor regions can be defined. Another current drawback is the requirement of performing calculations on a range of supercells for the purpose of the single parameter fit, increasing computational cost. This limitation may be overcome by using a more accurate functional (or higher-level theory than DFT) for the response calculation, provided that the unit cell is not so large as to make this computationally infeasible.

VI. CONCLUSIONS

In this work we have demonstrated the application of (linear-scaling) constrained DFT to charge-transfer states in the pentacene molecular crystal. Our results for isolated dimers are in reasonable agreement with higher-level theory calculations from the literature. Furthermore, we have used cluster calculations to illustrate the transition to the crystal limit, showing that CT energies are lowered both by screening and the formation of bands. We have devised a scheme based on periodic supercell calculations in combination with a dipole correction in order to establish the limit of the infinite molec-

ular crystal. Our dipole correction method is novel in that it is applicable to very general systems (non-cubic with anisotropic dielectric properties). It is also of significant interest that in spite of the high-polarity of the CT configurations, the excellent agreement between results for the cluster approximation and for the crystal limit reveals unexpectedly high screening capability for pentacene, with important consequences for the modelling of pentacene interfaces and film structural imperfections.

ACKNOWLEDGMENTS

DHPT and NDMH would like to gratefully acknowledge financial support from the Winton Programme for the Physics of Sustainability. In addition, DHPT gratefully acknowledges financial support from the Engineering and Physical Sciences Research Council, as well as access to computing resources provided by the Cambridge High Performance Computing Cluster *Darwin*. GT and DDO'R gratefully acknowledge the Royal Society and Royal Irish Academy for provision of an International Exchange grant. The underlying data of this publication can be accessed via the following persistent URI: <https://www.repository.cam.ac.uk/handle/1810/254222>

-
- [1] M. B. Smith and J. Michl, *Chem. Rev.* **110**, 6891 (2010).
- [2] M. B. Smith and J. Michl, *Annu. Rev. Phys. Chem.* **64**, 361 (2013).
- [3] J. Lee, P. Jadhav, P. D. Reusswig, S. R. Yost, N. J. Thompson, D. N. Congreve, E. Hontz, T. Van Voorhis, and M. A. Baldo, *Acc. Chem. Res.* **46**, 1300 (2013).
- [4] M. W. B. Wilson, A. Rao, J. Clark, R. S. S. Kumar, D. Brida, G. Cerullo, and R. H. Friend, *J. Am. Chem. Soc.* **133**, 11830 (2011).
- [5] A. Rao, M. W. B. Wilson, J. M. Hodgkiss, S. Albert-Seifried, H. Bässler, and R. H. Friend, *J. Am. Chem. Soc.* **132**, 12698 (2010).
- [6] W.-L. Chan, M. Ligges, A. Jailaubekov, L. Kaake, L. Miaja-Avila, and X.-Y. Zhu, *Science* **334**, 1541 (2011).
- [7] H. Marciniak, M. Fiebig, M. Huth, S. Schiefer, B. Nickel, F. Selmaier, and S. Lochbrunner, *Phys. Rev. Lett.* **99**, 176402 (2007).
- [8] H. Marciniak, I. Pugliesi, B. Nickel, and S. Lochbrunner, *Phys. Rev. B* **79**, 235318 (2009).
- [9] D. Beljonne, H. Yamagata, J. L. Brédas, F. C. Spano, and Y. Olivier, *Phys. Rev. Lett.* **110**, 226402 (2013).
- [10] T. C. Berkelbach, M. S. Hybertsen, and D. R. Reichman, *J. Chem. Phys.* **138**, 114103 (2013).
- [11] P. M. Zimmerman, F. Bell, D. Casanova, and M. Head-Gordon, *J. Am. Chem. Soc.* **133**, 19944 (2011).
- [12] P. M. Zimmerman, Z. Zhang, and C. B. Musgrave, *Nat. Chem.* **2**, 648 (2010).
- [13] T. Zeng, R. Hoffmann, and N. Ananth, *J. Am. Chem. Soc.* **136**, 5755 (2014).
- [14] D. N. Congreve, J. Lee, N. J. Thompson, E. Hontz, S. R. Yost, P. D. Reusswig, M. E. Bahlke, S. Reineke, T. V. Voorhis, and M. A. Baldo, *Science* **340**, 334 (2013).
- [15] A. A. Bakulin, S. E. Morgan, T. B. Kehoe, M. W. B. Wilson, A. W. Chin, D. Zigmantas, D. Egorova, and A. Rao, *Nat. Chem.* **8**, 16 (2016).
- [16] T. C. Berkelbach, M. S. Hybertsen, and D. R. Reichman, *J. Chem. Phys.* **138**, 114102 (2013).
- [17] T. C. Berkelbach, M. S. Hybertsen, and D. R. Reichman, *J. Chem. Phys.* **141**, 074705 (2014).
- [18] W.-L. Chan, T. C. Berkelbach, M. R. Provorse, N. R. Monahan, J. R. Tritsch, M. S. Hybertsen, D. R. Reichman, J. Gao, and X.-Y. Zhu, *Acc. Chem. Res.* **46**, 1321 (2013).
- [19] L. Sebastian, G. Weiser, and H. Bässler, *Chem. Phys.* **61**, 125 (1981).
- [20] L. Sebastian, G. Weiser, G. Peter, and H. Bässler, *Chem. Phys.* **75**, 103 (1983).
- [21] A. Dreuw, J. L. Weisman, and M. Head-Gordon, *J. Chem. Phys.* **119**, 2943 (2003).
- [22] Y. Tawada, T. Tsuneda, S. Yanagisawa, T. Yanai, and K. Hirao, *J. Chem. Phys.* **120**, 8425 (2004).
- [23] S. Sharifzadeh, A. Biller, L. Kronik, and J. B. Neaton, *Phys. Rev. B* **85**, 125307 (2012).
- [24] P. H. Dederichs, S. Blügel, R. Zeller, and H. Akai, *Phys. Rev. Lett.* **53**, 2512 (1984).
- [25] Q. Wu and T. Van Voorhis, *Phys. Rev. A* **72**, 024502 (2005).
- [26] Q. Wu and T. Van Voorhis, *J. Chem. Theory* **2**, 765 (2006).
- [27] B. Kaduk, T. Kowalczyk, and T. Van Voorhis, *Chem. Rev.* **112**, 321 (2012).
- [28] C.-K. Skylaris, P. D. Haynes, A. A. Mostofi, and M. C. Payne, *J. Chem. Phys.* **122**, 084119 (2005).
- [29] J. Řezáč and A. de la Lande, *J. Chem. Theory* **11**, 528 (2015).
- [30] V. Vaissier, J. M. Frost, P. R. F. Barnes, and J. Nelson, *J. Phys. Chem. C* **119**, 24337 (2015).
- [31] S. Zheng, H. Phillips, E. Geva, and B. D. Dunietz, *J. Am. Chem. Soc.* **134**, 6944 (2012).
- [32] S. Zheng, E. Geva, and B. D. Dunietz, *J. Chem. Theory* **9**, 1125 (2013).
- [33] A. Kubas, F. Hoffmann, A. Heck, H. Oberhofer, M. Elstner, and J. Blumberger, *J. Chem. Phys.* **140**, 104105 (2014).
- [34] A. Kubas, F. Gajdos, A. Heck, H. Oberhofer, M. Elstner, and J. Blumberger, *Phys. Chem. Chem. Phys.* **17**, 14342 (2015).
- [35] Y. Si, W. Liang, and Y. Zhao, *J. Phys. Chem. C* **116**, 12499 (2012).
- [36] K. Aikawa, M. Sumita, Y. Shimodo, and K. Morihashi, *Phys. Chem. Chem. Phys.* **17**, 20923 (2015).
- [37] T. J. Eisenmayer, J. A. Lasave, A. Monti, H. J. M. de Groot, and F. Buda, *J. Phys. Chem. B* **117**, 11162 (2013).
- [38] J. Yu, D. M. Huang, J. G. Shapter, and A. D. Abell, *J. Phys. Chem. C* **116**, 26608 (2012).

- [39] K. R. Siefermann, C. D. Pemmaraju, S. Neppl, A. Shavorskiy, A. A. Cordones, J. Vura-Weis, D. S. Slaughter, F. P. Sturm, F. Weise, H. Bluhm, M. L. Strader, H. Cho, M.-F. Lin, C. Bacellar, C. Khurmi, J. Guo, G. Coslovich, J. S. Robinson, R. A. Kaindl, R. W. Schoenlein, A. Belkacem, D. M. Neumark, S. R. Leone, D. Nordlund, H. Ogasawara, O. Krupin, J. J. Turner, W. F. Schlotter, M. R. Holmes, M. Messerschmidt, M. P. Minitti, S. Gul, J. Z. Zhang, N. Huse, D. Prendergast, and O. Gessner, *J. Phys. Chem. Letters* **5**, 2753 (2014).
- [40] J. Rezáč, B. Lévy, I. Demachy, and A. de la Lande, *J. Chem. Theory* **8**, 418 (2012).
- [41] H. Oberhofer and J. Blumberger, *J. Chem. Phys.* **131**, 064101 (2009).
- [42] S.-S. Sun and L. R. Dalton, *Introduction to Organic Electronic and Optoelectronic Materials and Devices* (CRC Press: New York, 2008).
- [43] S. R. Forrest, *Nature* **428**, 911 (2004).
- [44] Y. Zhao, Y. Guo, and Y. Liu, *Adv. Mater.* **25**, 5372 (2013).
- [45] W. J. M. Naber, S. Faez, and W. G. v. d. Wiel, *J. Phys. D* **40**, R205 (2007).
- [46] S. Baroni, S. de Gironcoli, A. Dal Corso, and P. Gianozzi, *Rev. Mod. Phys.* **73**, 515 (2001).
- [47] P. B. Coto, S. Sharifzadeh, J. B. Neaton, and M. Thoss, *J. Chem. Theory* **11**, 147 (2014).
- [48] C.-K. Skylaris, A. A. Mostofi, P. D. Haynes, O. Diéguez, and M. C. Payne, *Phys. Rev. B* **66**, 035119 (2002).
- [49] W. Kohn, "Nearsightedness of electronic matter," in *Proceedings of the Conference in Honor of C N Yang's 85th Birthday* (World Scientific, 2008) Chap. 18, pp. 217–217.
- [50] C.-K. Skylaris and P. D. Haynes, *J. Chem. Phys.* **127**, 164712 (2007).
- [51] D. D. O'Regan, N. D. M. Hine, M. C. Payne, and A. A. Mostofi, *Phys. Rev. B* **82**, 081102 (2010).
- [52] E. Artacho and L. Miláns del Bosch, *Phys. Rev. A* **43**, 5770 (1991).
- [53] D. D. O'Regan, N. D. M. Hine, M. C. Payne, and A. A. Mostofi, *Phys. Rev. B* **85**, 085107 (2012).
- [54] T. Ozaki, *Phys. Rev. B* **64**, 195110 (2001).
- [55] D. D. O'Regan, M. C. Payne, and A. A. Mostofi, *Phys. Rev. B* **83**, 245124 (2011).
- [56] L. E. Ratcliff, L. Grisanti, L. Genovese, T. Deutsch, T. Neumann, D. Danilov, W. Wenzel, D. Beljonne, and J. Cornil, *J. Chem. Theory* **11**, 2077 (2015).
- [57] L. E. Ratcliff, L. Genovese, S. Mohr, and T. Deutsch, *J. Chem. Phys.* **142**, 234105 (2015).
- [58] A. Ruiz-Serrano, N. D. M. Hine, and C.-K. Skylaris, *J. Chem. Phys.* **136**, 234101 (2012).
- [59] S. J. Clark, M. D. Segall, C. J. Pickard, P. J. Hasnip, M. I. J. Probert, K. Refson, and M. C. Payne, *Z. Kristallogr.* **220**, 567 (2005).
- [60] R. B. Campbell, J. M. Robertson, and J. Trotter, *Acta Crystallogr.* **15**, 289 (1962).
- [61] N. D. M. Hine, J. Dziedzic, P. D. Haynes, and C.-K. Skylaris, *J. Chem. Phys.* **135**, 204103 (2011).
- [62] P. P. Ewald, *Ann. Phys.* **369**, 253 (1921).
- [63] G. Makov and M. C. Payne, *Phys. Rev. B* **51**, 4014 (1995).
- [64] M. Leslie and N. J. Gillan, *J. Phys. C: Solid State Phys.* **18**, 973 (1985).
- [65] K. P. McKenna and J. Blumberger, *Phys. Rev. B* **86**, 245110 (2012).
- [66] J. Blumberger and K. P. McKenna, *Phys. Chem. Chem. Phys.* **15**, 2184 (2013).
- [67] S. T. Murphy and N. D. M. Hine, *Phys. Rev. B* **87**, 094111 (2013).
- [68] L. N. Kantorovich, *Phys. Rev. B* **60**, 15476 (1999).
- [69] G. Fischerauer, *IEEE Trans. Ultrason. Ferroelect., Freq. Control* **44**, 1179 (1997).
- [70] G. Lever, D. J. Cole, N. D. M. Hine, P. D. Haynes, and M. C. Payne, *J. Phys. Condens. Matter* **25**, 152101 (2013).
- [71] M. L. Tiago, J. E. Northrup, and S. G. Louie, *Phys. Rev. B* **67**, 115212 (2003).
- [72] P. Cudazzo, M. Gatti, and A. Rubio, *Phys. Rev. B* **86**, 195307 (2012).
- [73] S. Sharifzadeh, P. Darancet, L. Kronik, and J. B. Neaton, *J. Phys. Chem. Letters* **4**, 2197 (2013).